Mon. Not. R. Astron. Soc. **000**, 1–7 (2008) Printed 2 November 2012 (MN LaTeX style file v2.2)

arXiv:1211.0088v1 [astro-ph.CO] 1 Nov 2012

Effects of photon trapping on the Lyα properties of star-forming galaxies

Hidenobu Yajima[1,2]⋆ and Yuexing Li[1,2]
[1] *Department of Astronomy and Astrophysics, Pennsylvania State University, 525 Davey Lab, University Park, PA 16802, USA*
[2] *Institute for Gravitation and the Cosmos, The Pennsylvania State University, University Park, PA 16802, USA*

Accepted ?; Received ??; in original form ???

ABSTRACT

Recent observations show that a large number of Lyman-alpha emitters (LAEs) at high redshift $z \gtrsim 3$ have unusually high Lyα equivalent widths (EW $\gtrsim 400$ Å). However, the origin of these high EWs is an open question. Here, we investigate the impacts of photon trapping on the Lyα EW and other properties by tracking the Lyα radiative transfer in spherical galactic clouds. We find that the delayed escape of the Lyα photons can change the Lyα properties significantly. During the transition phase from optically thick to optically thin where the Lyα photons can escape simultaneously, the EW can be boosted to ~ 1000 Å, the Lyα luminosity can be increased by a factor of a few, and the line profile can be significantly broadened. The boost factor appears to depend on the galaxy properties such as mass and star formation rate and timescale, therefore future investigation combing 3D Lyα RT calculations with cosmological simulations of galaxy formation and evolution is needed to fully understand the Lyα properties of early star-forming galaxies.

Key words: radiative transfer – galaxies: evolution – galaxies: formation – galaxies: high-redshift

1 INTRODUCTION

The hydrogen Lyα line has played an important role in detecting distant galaxies. To date, a large population of Lyα emitters (LAEs) have been observed at high redshifts $z \gtrsim 3$ (e.g., Hu & McMahon 1996; Cowie & Hu 1998; Iye et al. 2006; Gawiser et al. 2006; Gronwall et al. 2007; Lai et al. 2008; Ouchi et al. 2008; Lehnert et al. 2010; Kashikawa et al. 2012; Shibuya et al. 2012). One of the important properties of Lyα is the equivalent width (EW), which measures the ratio of Lyα flux to that of the UV continuum, and therefore provides useful information of the emission mechanisms and photon escape processes in galaxies.

Unlike UV continuum, Lyα photons typically experience many scattering process in galaxies due to its large scattering cross section. These scatterings may prolong the path length and increase the probability of dust absorption, leading to reduction in the emergent luminosity. Hence, the EW can change significantly due to the difference in the radiative transfer (RT) process between Lyα and UV continuum. If the escape fraction of Lyα is the same as that of the UV continuum, the upper limit of the EW is determined by the intrinsic spectral energy distribution (SED) of the stars. It has been suggested that in the case of a Salpeter initial mass function (IMF), the upper limit is ~ 400 Å (e.g., Schaerer 2003).

However, a large number of LAEs at $z \gtrsim 3$ have large EWs higher than 400 Å (e.g., Gronwall et al. 2007; Ouchi et al. 2008). More recently, Kashikawa et al. (2012) detected a LAE with extremely large EW of ~ 900 Å at $z = 6.5$. The origin of such high EWs is largely unknown.

It has been proposed that the large EWs may be produced by a top-heavy IMF of PopIII stars (e.g., Gronwall et al. 2007; Kashikawa et al. 2012). However, so far there is no evidence of a top-heavy IMF in high-redshift LAEs (e.g., Nagao et al. 2008), or a PopIII-dominated galaxy. Another model used a Salpeter IMF but invoked clumpy interstellar medium (Neufeld 1991; Hansen & Oh 2006). In this model, UV continuum is assumed to be absorbed by dust passing through the dense clouds, but Lyα photons do not experience the dust absorption because they cannot enter the clouds due to surface scattering. However, this is an idealized, optically thin case for the Lyα photons. In fact, most of the stars form in high density clouds, they ionize the gas and create H$_{\rm II}$ regions which emit Lyα photons. These photons then travel in the dense clouds and may experience strong dust extinction. Recently, Yajima et al.

⋆ E-mail: yuh19@psu.edu(HY);

© 2008 RAS

(2012b) studied the escape of Lyα and continuum photons from star-forming galaxies by combining a cosmological simulation with three-dimensional radiative transfer calculations, and found no correlation between the EW and clumpiness of the ISM. Furthermore, using the same simulations, Yajima et al. (2012c) found that collisional excitation from accretion of cold hydrogen gas by a galaxy at high redshift ($z \gtrsim 6$) significantly enhance the Lyα emission and boost the EW.

It is not clear, however, from our previous studies whether or not cold accretion is the only dominant mechanism to produce a large EW. In many RT calculations, all Lyα photons were assumed to escape instantaneously with the UV continuum. However, since the ionization of hydrogen evolves with time, this time-dependent propagation of the ionization front may cause a delay of the escape of the Lyα photons (Pierleoni et al. 2009), which in turn may affect the Lyα properties. However, the time evolution of ionization has not been considered in most Lyα RT calculations before.

In this work, we consider the pure effects of photon trapping on the Lyα properties. We perform full Lyα RT, which includes time-evolving ionization structure, in spherical galactic clouds, and track the resulting Lyα EW, luminosity, and line profiles. The paper is organized as follows: in § 2 we describe our galaxy models and RT methods, in § 3 we present the results of the Lyα properties, we discuss our model assumptions and parameters in § 4, and summarize in § 5.

2 METHODOLOGY

2.1 Galaxy Models

Our galaxy model consists of one-dimensional spherical shells of hydrogen gas in a spherical Navarro-Frenk-White dark matter halo (Navarro et al. 1997), similar to that of Dijkstra & Loeb (2009). The dark matter halo has a concentration parameter $c = 3.8$ (Gao et al. 2008) at the virial temperature of the halo as derived by Makino et al. (1998) at $z_{\rm vir} = 3$. The gas is assumed to be in hydrostatic equilibrium and isothermal, with a temperature of $T = 10^4$ K, as suggested by Dijkstra & Loeb (2009). A total of 100 shells are constructed for each galaxy.

In addition, we assume star formation takes place at the center of the galaxy, with the rate SFR proportional to the halo mass (e.g., Trac & Cen 2007), and decays exponentially,

$$\mathrm{SFR}(t) = f_{\rm SFR} \left(\frac{M_h}{10^{10}\ M_\odot}\right) \exp\left(-\frac{t}{\tau_{\rm SFR}}\right) \qquad (1)$$

where $f_{\rm SFR}$ and $\tau_{\rm SFR}$ are amplitude factor of peak SFR and star formation timescale respectively. In this work, the $f_{\rm SFR}$ and $\tau_{\rm SFR}$ are free parameters with a range $f_{\rm SFR} = 0.05 - 5.0$ and $\tau_{\rm SFR} = 5 \times 10^6 - 10^8$ yr.

Along with the star formation history, newly formed stars are added to the galaxy center. We estimate the number of ionizing photons from stacked SEDs. The SED is calculated by summing that star clusters are created in each time step. We use PEGASE ver.2.0 (Fioc & Rocca 1997) to calculate the SEDs and assume a metallicity of $Z = 0.05 Z_\odot$. In each time step, we estimate the ionization structure from the balance between recombination and photo-ionization,

$$\dot{N}_{\rm ion} = \int_0^{R_{\rm i}} 4\pi r'^2 \alpha_{\rm B} n_{\rm HII}(r) n_{\rm e}(r) dr' \qquad (2)$$

where $\dot{N}_{\rm ion}$, $R_{\rm i}$, $\alpha_{\rm B}$ are the emissivity of ionizing photons, the radius of ionized region and the recombination rate to all excitation state, respectively. The gas at $r \leqslant R_{\rm i}$ is completely ionized region, while at $r > R_{\rm i}$ it is in neutral state.

2.2 Radiative Transfer

The RT calculations are performed using the 3D Monte Carlo RT code, All-wavelength Radiative Transfer with Adaptive Refinement Tree (ART^2) (Li et al. 2008; Yajima et al. 2012a). The multi-wavelength continuum emission of ART^2 is described in Li et al. (2008), while the implementation of Lyα line transfer is detailed in Yajima et al. (2012a). Here we focus on the RT of Lyα photons in the ionization structure of the galactic shells and briefly outline the process.

In the Lyα RT, it is important to calculate the frequency change due to the scattering process. In the scattering process, the final frequency in the laboratory frame is then:

$$\frac{\nu^{\rm out} - \nu_0}{\Delta\nu_{\rm D}} = \frac{\nu^{\rm in} - \nu_0}{\Delta\nu_{\rm D}} - \frac{V_{\rm a} \cdot k_{\rm in}}{V_{\rm th}} + \frac{V_{\rm a} \cdot k_{\rm out}}{V_{\rm th}} \qquad (3)$$

where, $\nu^{\rm in}$ and $\nu^{\rm out}$ are incoming and outgoing frequency in the rest frame of scattering medium, respectively, the line center frequency $\nu_0 = 2.466 \times 10^{15}$ Hz, $\Delta\nu_{\rm D} = (V_{\rm th}/c)\nu_0$ corresponds to the Doppler frequency width and $V_{\rm th}$ is the velocity dispersion of the Maxwellian distribution describing the thermal motions, i.e., $V_{\rm th} = (2k_{\rm B}T/m_{\rm H})^{1/2}$, $V_{\rm a}$ is the atom velocity, $k_{\rm in}$ and $k_{\rm out}$ are incoming and outgoing propagation direction respectively.

Unlike continuum photons, the Lyα photons can experience many scattering processes, which lead to long path length and long scattering timescale before the photons escape. As a result, the ionization structure may change while the photons are traveling. Here, we consider the change of ionization structure with time in the Lyα RT process. The optical depth is estimated to be $d\tau = \sigma_\nu n_{\rm HI}(i,j) ds$, where i and j are indexes of the shell position and the time step, respectively. In each scattering, if the traveling of the Lyα moves to the next time step, the ionization structure of that time step is used to estimate the optical depth.

The intrinsic Lyα luminosity is estimated as:

$$L_\alpha = 0.68 h\nu_\alpha \dot{N}_{\rm ion}(1 - f_{\rm esc}^{\rm ion}) \qquad (4)$$

where ν_α and $f_{\rm esc}^{\rm ion}$ are the Lyα frequency and the escape fraction of ionizing photons, respectively. The start point of the photon package is randomly chosen with the weight by the Lyα emissivity of each spherical shell, $\epsilon_\alpha^i \propto \pi(r_i^3 - r_{i-1}^3) n_{\rm HII}^i n_{\rm e}^i$, where i is the shell index.

A total of 128 photon packets are used at each time step. Each packet has a energy which is the L_α at the time step divided by the packet number. The initial frequency is randomly chosen from a Gaussian distribution.

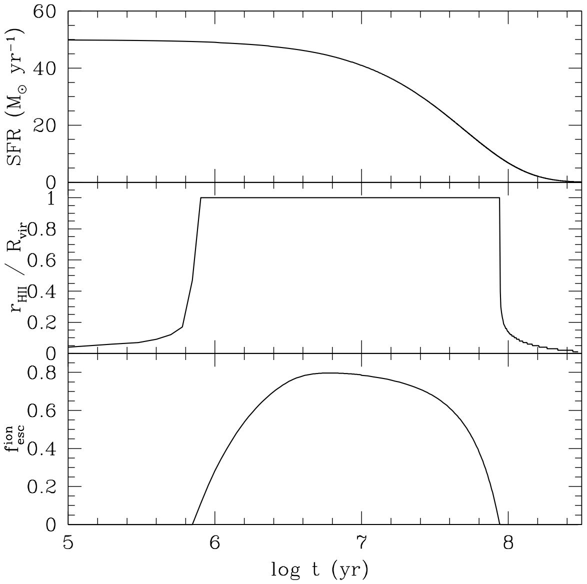

Figure 1. Time evolution of the SFR (*upper panel*), size of the ionization front normalized by the virial radius (*middle panel*), and the escape fraction of ionizing photons (*lower panel*), for a galaxy with mass $M_{\rm tot} = 10^{12}\ M_\odot$, and fiducial parameters star formation timescale $\tau_{\rm SFR} = 5 \times 10^7$ yr, and star formation amplitude factor $f_{\rm SFR} = 0.5$.

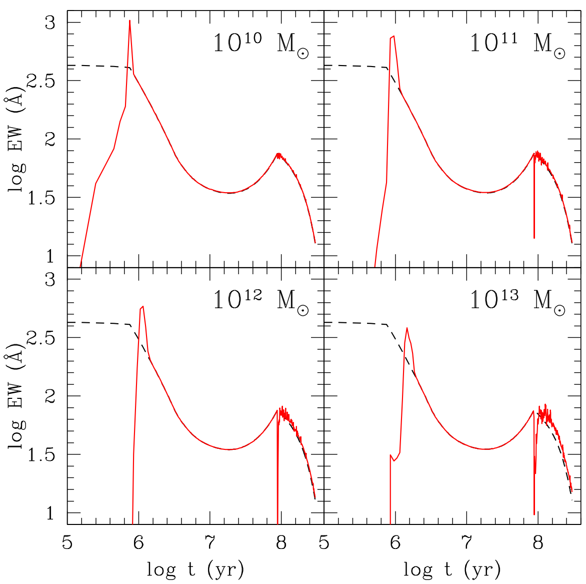

Figure 2. Time evolution of the Lyα EW for 4 different galaxies with mass of $10^{10}\ M_\odot$ (upper left panel), $10^{11}\ M_\odot$ (upper right panel), $10^{12}\ M_\odot$ (lower left panel), $10^{13}\ M_\odot$ (lower right panel), respectively. Fiducial parameters $f_{\rm SFR} = 0.5$ and $\tau_{\rm SFR} = 5 \times 10^7$ yr are used for all galaxies. The red solid line is the resulting EW from our model which takes into account the trapping of Lyα photons due to the time evolution of ionization structure in the galaxy, while the black dashed line is the predicted EW assuming that all Lyα photons escape instantaneously. A Salpeter IMF is assumed in these calculations.

3 RESULTS

3.1 Ionization History

Figure 1 shows the evolution of the star formation rate, the size of the ionized region, and the escape fraction of ionizing photons $f_{\rm esc}^{\rm ion}$ with time for a galaxy with mass $M_{\rm tot} = 10^{12}\ M_\odot$, a star formation timescale $\tau_{\rm SFR} = 5 \times 10^7$ yr, and a star formation amplitude factor $f_{\rm SFR} = 0.5$. The SFR has an initial value of 50 M$_\odot$ yr^{-1}, but exponentially decreases with time. Since ionizing photons mainly come from massive, young stars, they are strongly correlated with SFR. As a result, in the early phase ($t \lesssim 6 \times 10^7$ yr), the ionizing front reaches the $R_{\rm vir}$. Then, the ionization front steeply decreases with SFR, and becomes $\sim 0.1 R_{\rm vir}$ at $\sim 10^8$ yr.

In the current model of ionization, the $f_{\rm esc}$ of ionizing photons becomes > 0 when all gas in the galaxy is ionized. Therefore, the $f_{\rm esc}$ is nonzero at $t \lesssim 6 \times 10^7$ yr. It starts from ~ 0.6, then decreases with SFR. When all gas is ionized, the $f_{\rm esc}$ is estimated by $(1 - \dot{N}_{\rm rec,tot})/\dot{N}_{\rm ion}$, where $\dot{N}_{\rm rec,tot}$ is the number of total recombination hydrogen. Since the $\dot{N}_{\rm rec,tot}$ is time-independent, therefore the $f_{\rm esc}$ is correlated with SFR.

3.2 Lyα Equivalent Width

We estimate the EW in rest frame from $EW = L_\alpha / L_\lambda^{\rm UV}$, where $L_\lambda^{\rm UV}$ is luminosity density of UV continuum, here we use the luminosity density at 1400 Å. Figure 2 shows the resulting time evolution of EWs with the fiducial values $f_{\rm SFR} = 0.5$ and $\tau_{\rm SFR} = 5 \times 10^7$ yr, for 4 different galaxies in the mass range of $10^{10-13}\ M_\odot$.

At first, the ionized region is confined in the galaxy, then it grows with increasing stellar mass. In this phase, the Lyα photons are also confined in the galaxy, hence the EW is very small. However, when the ionization front reaches the virial radius, the trapped Lyα photons can escape simultaneously. This sudden release of Lyα photons causes very high EWs, which peaks $\sim 400 - 1000$ Å, much higher than the upper limit predicted by the model in which all Lyα photons escape instantaneously.

Moreover, the peak of EW decreases with increasing halo mass. In small galaxies, the potential well is shallow, the SFR is low, and the virial radius $R_{\rm vir}$ is small, therefore it is easy for the ionization to propagate and reach $R_{\rm vir}$ quickly. Meanwhile, low SFR produces low UV continuum flux, so the resulting Lyα EW is high. In contrast, more massive galaxies have larger virial radius, so the time it takes for the ionization front to reach $R_{\rm vir}$ is longer, and the higher SFR produces higher UV continuum flux, which results in smaller Lyα EW. In addition, in the larger radius, the traveling time from last scattering to escape can change depending on the position and angle, resulting in the extended and smaller peak of EW.

Once the galaxy is ionized, the ionizing photons can escape, and the escape fraction is fixed. From Equations (2) and (4), the intrinsic Lyα luminosity then becomes constant, $L_\alpha = 0.68 h\nu_\alpha \int_0^{R_{\rm vir}} 4\pi r^2 \alpha_{\rm B} n_{\rm H}^2(r) dr$. On the other hand, the UV continuum can continue to increase with the formation of new stars. Thus, upon completion of ionization, the intrinsic Lyα luminosity decreases relatively to UV continuum, resulting in a decrease of Lyα EW.

After that, however, the ionized region is confined within $R_{\rm vir}$ again due to decreased SFR. Most of Lyα photons are trapped within the galaxy by the neutral hydrogen shell. Some of the trapped photons can escape through scattering and random processes, leading to a mild increase of the EW. However, the UV continuum slowly catches up again with new star formation, bringing down the EW.

The interplay between Lyα and UV continuum photons in the RT processes results in a unique saddle-like shape of the EW as a function of time. To better understand the oscillatory behavior of the EW, we illustrate in Figure 3 a schematic cartoon of the time evolution of the ionization structure and the escape of Lyα photons. There are four major phases in the evolution which affect the Lyα EW significantly:

(a): Early phase when the ionized region is confined in the galaxy due to low SFR and stellar mass. Most of the Lyα photons are trapped in the galaxy. The resulting Lyα EW is very small.
(b): As more stars form, the flood of ionizing photons from young, massive stars quickly ionizes the galaxy. The previously trapped Lyα photons as well as the new ones created via recombination of the ionizing photons in the HII regions escape instantaneously, causing a sudden and strong boost of the EW.
(c): With the decline of SFR due to ionization, the number of ionizing photons is reduced, and the ionized region is confined in the galaxy again. The cooled and neutral hydrogen can trap the Lyα photons, leading to a decrease of the EW.
(d): As the stars become older and dimmer, the UV continuum flux decreases. Meanwhile, some of the trapped Lyα photons escape after some scatterings. Hence, the Lyα luminosity increases relatively to the UV continuum, bringing a rise of the EW again.

3.3 Lyα Luminosity

Owing to the time-dependence of the ionization structure, the emergent Lyα luminosity (L_α) from the galaxy evolves with time as well. Figure 4 shows the corresponding L_α from the modeled galaxies as a function of time.

During Phase (a), the Lyα photons are trapped in the galaxy, the L_α approaches to zero in the modeled galaxies. As the galaxy gradually becomes optically thin due to ionization, Lyα photons can escape, steadily increasing the luminosity. Upon Phase (b) when the galaxy is completely ionized, all the Lyα photons, including both the previously trapped and the newly created ones, escape instantaneously, resulting in a drastic, strong peak of the L_α. After that, the ionized region is confined in the galaxy, the Lyα photons are trapped again as in Phase (c) and (d). But since the Lyα photons escape mainly through scattering, the fraction remains nearly constant during these phases, leading to constant luminosity. At the end of the star formation timescale, no more new stars form, the number of ionizing and Lyα photons declines sharply, so the galaxy becomes optically thick, and most of the Lyα photons become trapped, resulting in a rapid drop of the luminosity.

The evolution of the Lyα luminosity does not show the characteristic "saddle" shape as the EW. This is because the Lyα luminosity depends only on the ionization structure and the escaping process, it does not depend strongly on the UV continuum as does the EW.

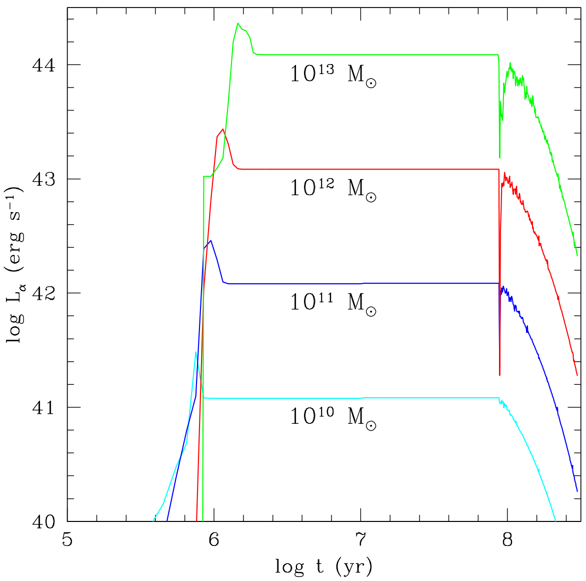

Figure 4. Evolution of emergent Lyα luminosity from the four modeled galaxies as indicated by the colors (cyan : $M_{\rm tot} = 10^{10}\ M_\odot$, blue : $M_{\rm tot} = 10^{11}\ M_\odot$, red : $M_{\rm tot} = 10^{12}\ M_\odot$ and green : $M_{\rm tot} = 10^{13}\ M_\odot$).

In contrast to the EW, which in general decreases with galaxy mass, the Lyα luminosity increases with galaxy mass. This is because both the SFR and the total recombination number are proportional to the galaxy mass, and as a result, the L_α increases linearly with the galaxy mass.

3.4 Lyα Line Profiles

Figure 5 shows the emergent line profiles from the model which takes into account the delayed escape of Lyα photons due to the time-depdendence of the ionization structure in the galaxy, in comparison with those without photon trapping.

At $t = 6.5 \times 10^5$ yr, which corresponds to Phase (a) in Figure 3, the delayed-escaping model predicts that the Lyα photons are trapped in the galaxy, there is no emergent line emission. In contrast, the instantaneous-escaping model predicts a double-peak profile caused by scattering of the neutral shells. At Phase (b) when the galaxy is completely ionized ($t = 1.2 \times 10^6$ yr), the galaxy becomes optically thin. The line profile without the time dependence shows a narrow profile peaking around $x = 0$, which is the intrinsic profile, while the line from the trapping model shows not only the central peak, but also a significantly extended distribution in both the blue and red wings. The broadening is caused by the scatterings of the trapped photons before they escape. Then, in Phase (c) ($t = 9.0 \times 10^7$ yr), the galaxy becomes optically thick again, the line profile thus shows double peak owing to scattering, and the luminosity from the trapping model is lower than that from the no-trapping model as expected. In Phase (d) ($t \sim 1.3 \times 10^8$ yr), with the decline of SFR, the size of the ionized region becomes small. As a re-

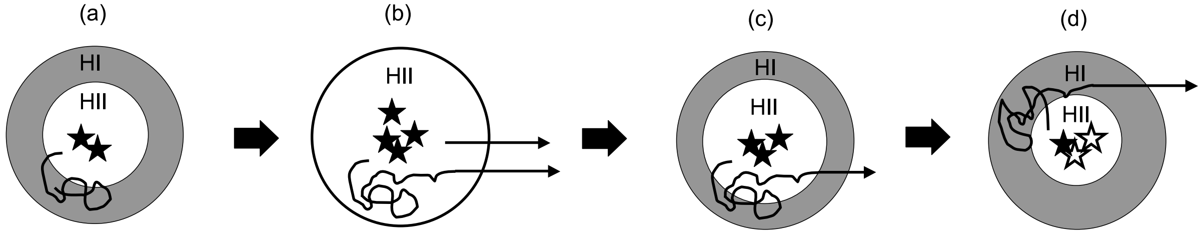

Figure 3. Schematic view of the interplay between ionization and Lyα escaping as a function of time. (a): the ionized region is confined in the galaxy, the Lyα photons are trapped. (b): the galaxy is completely ionized, the accumulated Lyα photons escape instantaneously. (c): the ionized region is confined again, and the Lyα photons are trapped again. (d): the stars become older and dimmer, some Lyα photons escape through scattering.

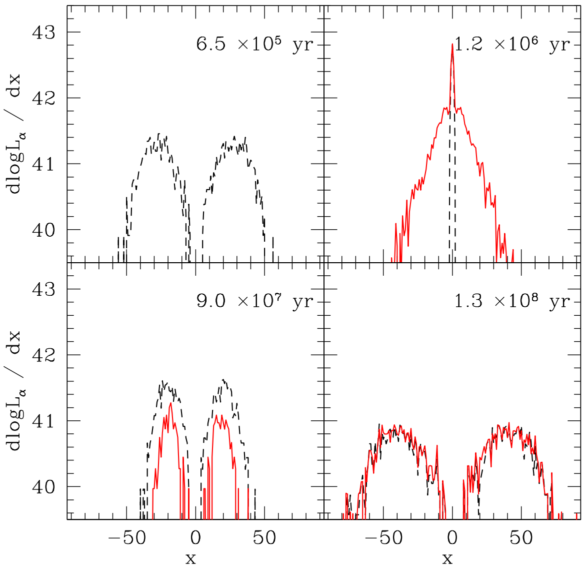

Figure 5. The Lyα line profile of the $M_{\rm tot} = 10^{12}\ M_\odot$ galaxy at four different times: $t = 6.5\times10^5, 1.2\times10^6, 9.0\times10^7$ and 1.3×10^8 yr, respectively. Fiducial parameters star formation timescale $\tau_{\rm SFR} = 5\times10^7$ yr, and star formation amplitude factor $f_{\rm SFR} = 0.5$ are used. The red solid line is the line profile from our model which takes into account the trapping of Lyα photons due to the time evolution of ionization structure in the galaxy, while the black dashed line is the predicted profile assuming that all Lyα photons escape instantaneously. The x is frequency shift in Doppler units, $x = (\nu - \nu_0)/\Delta\nu_{\rm D}$.

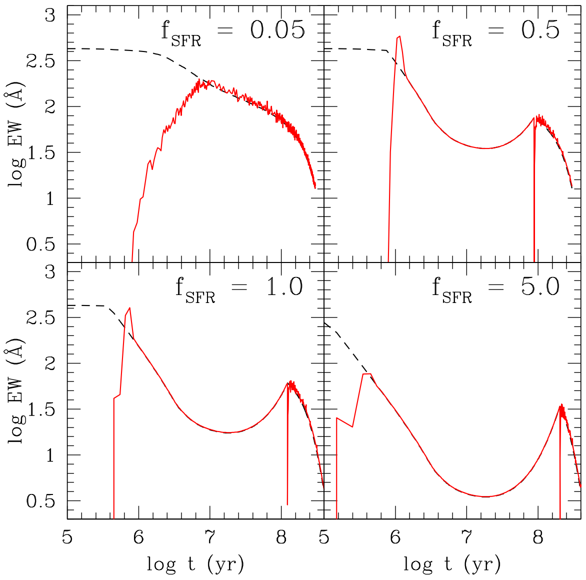

Figure 6. The EW with different amplitude factor of SFR as a function of evolution time. The total mass of galaxy is $10^{12}\ M_\odot$ and $\tau_{\rm SFR} = 5\times10^7$ yr. Black dash lines are the EW in the assumption that all Lyα photons instantaneously escape. Red solid lines are the EW considering the time evolution of ionization structure while Lyα photons travel in the galaxy.

sult, the optical depth from the center to the $R_{\rm vir}$ increases, the distance between the peaks in the profile thus increases, resulting in two broad double peaks.

4 DISCUSSIONS

In our model, there are two free parameters, the amplitude factor of peak SFR, $f_{\rm SFR}$, and star formation timescale, $\tau_{\rm SFR}$. In the previous sections, we have presented results using the fiducial numbers $f_{\rm SFR} = 0.5$ and $\tau_{\rm SFR} = 5\times10^7$ yr. Here we explore the dependence of our results on these two parameters.

Figure 6 shows the EW with difference $f_{\rm SFR}$ for the galaxy with $M_{\rm tot} = 10^{12}\ M_\odot$ and $\tau_{\rm SFR} = 5\times10^7$ yr. For $f_{\rm SFR} = 0.05$, the ionized region is always confined in the galaxy owing to low SFR. Hence, there is no EW peak even at the Phase (b) in figure 3. The EW simply decreases with SFR as the mean stellar age becomes old. For $f_{\rm SFR} \sim 0.5 - 1.0$, there is a EW peak at Phase (b). With higher $f_{\rm SFR}$, however, both the SFR and the mass of young stars are higher, leading to an earlier completion of ionization and higher UV continuum flux, which results in smaller EW.

Figure 7 shows the EW with different $\tau_{\rm SFR}$ for the galaxy with $M_{\rm tot} = 10^{12}\ M_\odot$ and $f_{\rm SFR} = 0.5$. All plots show significantly boosted EW peak at Phase (b), and similar "saddle" shape of the evolution of EW. The difference among these models lies in the duration of Phase (c). With shorter $\tau_{\rm SFR}$, the the occurrence of Phase (b) is more sig-

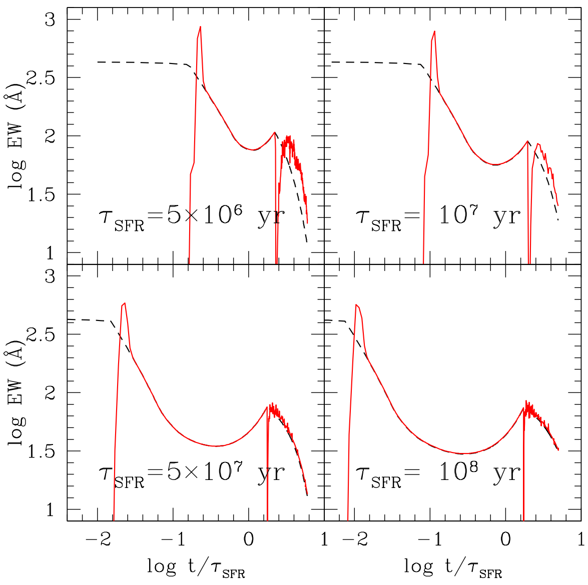

Figure 7. The EW with different time scale of star formation as a function of evolution time. The total mass of galaxy is 10^{12} $M_\odot$ and $f_{\rm SFR} = 0.5$. Black dash lines are the EW in the assumption that all Lyα photons instantaneously escape. Red solid lines are the EW considering the time evolution of ionization structure while Lyα photons travel in the galaxy.

nificantly delayed, resulting in larger difference in the EW evolution between the trapping and non-trapping models.

These results suggest that the EW depend sensitively on the galaxy properties such as star formation rate and timescale. In order to fully address the origin and nature of the EW distribution in LAEs, it is desired to combine 3D Lyα RT calculations with full cosmological simulations which include more realistic treatments of star formation and feedback processes, which we plan to do in future work.

5 SUMMARY

We have performed a set of Lyα RT calculations on idealized spherical galaxies to study the effects of photon trapping on the Lyα properties in star-forming galaxies, by taking into account the time dependence of the ionization process. We have identify four major phases in the evolution of the galaxy in our model:

- Phase (a): The ionized region is confined in the galaxy due to low SFR and stellar mass. Most of the Lyα photons are trapped in the galaxy, no emergent Lyα emission is observed.
- Phase (b): The galaxy is completely ionized. The previously trapped Lyα photons as well as the new ones created via recombination escape instantaneously, resulting in a dramatic and strong boost of the EW and luminosity, and a broadened line profile.
- Phase (c): The ionized region is confined in the galaxy again due to decrease of SFR and ionizing photons. The Lyα photons are trapped again, leading to a decrease of the EW and luminosity.
- Phase (d): The ionized region becomes smaller, as the stars become older and dimmer. The escape of the trapped Lyα photons is dominated by the stochastic scattering process. There is a small enhancement of the EW due to the decrease of the UV continuum flux, but the Lyα luminosity remains constant until the galaxy becomes strongly optically thick and trap most of the photons.

Our model suggests that the interplay between time-dependent ionization and Lyα scattering impacts significantly the Lyα EW, the emergent luminosity, and the line profile. During the transition phase from optically thick to optically thin where the Lyα photons can escape simultaneously, the EW can be boosted to $\sim$ 1000 Å, the Lyα luminosity can be increased by a factor of a few, and the line profile can be significantly broadened. These results may be able to explain the unusually large EW in some observed LAEs. However, the boost factor depends on the galaxy properties such as mass and star formation rate and timescale, future investigation combing 3D Lyα RT calculations with cosmological simulations of galaxy formation and evolution is needed to fully address this issue.

ACKNOWLEDGMENTS

We thank Masakazu A. R. Kobayashi, Tom Abel and Masayuki Umemura for stimulating discussions and helpful comments. Support from NSF grants AST-0965694 and AST-1009867 is gratefully acknowledged. We acknowledge the Research Computing and Cyberinfrastructure unit of Information Technology Services at The Pennsylvania State University for providing computational resources and services that have contributed to the research results reported in this paper (URL: http://rcc.its.psu.edu). The Institute for Gravitation and the Cosmos is supported by the Eberly College of Science and the Office of the Senior Vice President for Research at the Pennsylvania State University.

REFERENCES

Cowie L. L., Hu E. M., 1998, AJ, 115, 1319
Dijkstra M., Loeb A., 2009, MNRAS, 400, 1109
Fioc M., Rocca V. B., 1997, A& A, 326, 950
Gao L., Navarro J. F., Cole S., Frenk C. S., White S. D. M., Springel V., Jenkins A., Neto A. F., 2008, MNRAS, 387, 536
Gawiser E. et al., 2006, ApJ, 642, L13
Gronwall C. et al, 2007, ApJ, 667, 79
Hansen M., Oh S. P., 2006, MNRAS, 367, 979
Hu E. M., McMahon R. G., 1996, Nature, 382, 231
Iye M. et al., 2006, Nature, 443, 186
Kashikawa N. et al., 2012, ArXiv e-prints
Lai K. et al., 2008, ApJ, 674, 70
Lehnert M. D. et al., 2010, Nature, 467, 940
Li Y., Hopkins P. F., Hernquist L., Finkbeiner D. P., Cox T. J., Springel V., Jiang L., Fan X., Yoshida N., 2008, ApJ, 678, 41
Makino N., Sasaki S., Suto Y., 1998, ApJ, 497, 555
Nagao T. et al., 2008, ApJ, 680, 100
Navarro J. F., Frenk C. S., White S. D. M., 1997, ApJ, 490, 493

Neufeld D. A., 1991, ApJ, 370, L85
Ouchi M. et al., 2008, ApJS, 176, 301
Pierleoni M., Maselli A., Ciardi B., 2009, MNRAS, 393, 872
Schaerer D., 2003, A&A, 397, 527
Shibuya T., Kashikawa N., Ota K., Iye M., Ouchi M., Furusawa H., Shimasaku K., Hattori T., 2012, ApJ, 752, 114
Trac H., Cen R., 2007, ApJ, 671, 1
Yajima H., Li Y., Zhu Q., Abel T., 2012a, MNRAS, 424, 884
Yajima H., Li Y., Zhu Q., Abel T., Gronwall C., Ciardullo R., 2012b, MNRAS, submitted, arXiv: 1209.5842
—, 2012c, ApJ, 754, 118